MNRAS 000, 1–11 (2019) Preprint 27 November 2021 Compiled using MNRAS LATEX style file v3.0

Modelling the spectral energy distribution of super-Eddington quasars

Aya Kubota[1,2]⋆ and Chris Done[2]
[1]Department of Electronic Information Systems, Shibaura Institute of Technology, 307 Fukasaku, Minuma-ku, Saitama-shi, Saitama 337-8570, Jap
[2]Department of Physics, University of Durham, South Road, Durham, DH1 3LE, UK

arXiv:1905.02920v3 [astro-ph.GA] 29 Aug 2019

Accepted XXX. Received YYY; in original form ZZZ

ABSTRACT

We develop a broadband spectral model, AGNSLIM, to describe super-Eddington black hole accretion disc spectra. This is based on the slim disc emissivity, where radial advection keeps the surface luminosity at the local Eddington limit, resulting in $L(r) \propto r^{-2}$ rather than the r^{-3} expected from the Novikov-Thorne (standard, sub-Eddington) disc emissivity. Wind losses should also be important but these are expected to produce a similar radiative emissivity. We assume that the flow is radially stratified, with an outer standard disc, an inner hot Comptonising region and an intermediate warm Comptonising region to produce the soft X-ray excess. This gives the model enough flexibility to fit the observed data, but with the additional requirement of energy conservation to give physical constraints. We use this to fit the broadband spectrum of one of the most extreme Active Galactic Nuclei, the Narrow Line Seyfert 1 RX J0439.6 – 5311, which has a black hole mass of $(6 \sim 9) \times 10^6 M_\odot$ as derived from the Hβ line width. This cannot be fit with the standard disc emissivity at this mass, as even zero spin models overproduce the observed luminosity. Instead, we show that the spectrum is well reproduced by the slim disc model, giving mass accretion rates around (5 ∼ 10)×Eddington limit. There is no constraint on black hole spin as the efficiency is reduced by advection. Such extreme accretion rates should be characteristic of the first Quasars, and we demonstrate this by fitting to the spectrum of a recently discovered super-Eddington Quasar, PSO J006 + 39, at $z = 6.6$.

Key words: black hole physics – galaxies: Seyfert – accretion, accretion discs

1 INTRODUCTION

Active galactic Nuclei (AGN) are observed to shine at super-Eddington accretion rates. This is not immediately apparent from using a constant bolometric correction factor for the optical emission (e.g., Steinhardt & Elvis 2010). However, the accretion disc equations do not predict a constant bolometric correction factor as the maximum disc temperature increases with increasing mass accretion rate. Instead, these give $L_{\rm opt} \propto (M\dot{M})^{2/3} \propto (ML_{\rm bol})^{2/3}$ (Collin & Kawaguchi 2004; Davis & Laor 2011). Collin & Kawaguchi (2004) used this to show that some Narrow Line Seyfert 1 (NLS1) AGN had optical spectra which implied that their mass accretion rate was up to 10 times Eddington limit. Schulze et al. (2017) derive the Eddington ratio from a large sample of AGN using both techniques, and show that the disc equations transform the distribution from having a clear maximum at Eddington limit to extending significantly above Eddington limit. This observational support for exceeding the Eddington limit is important as the discovery of quasars with black hole masses of $\sim 10^9 M_\odot$ at $z > 7$ (e.g. Mortlock et al. 2011; Bañados et al. 2018) puts stringent constraints on the mass of the initial black hole seed. There is not enough time for such massive black holes to grow from even $100 M_\odot$ pop III stellar remnants by Eddington limited accretion for any reasonable black hole spin (Shapiro 2005). Either the seed black holes are more massive, though how these could form is not yet clear (e.g. Boekholt et al. 2018; Wise et al. 2019) or super-Eddington rates are required.

However, merely having a super-Eddington luminosity does not necessarily mean that the black hole can accrete all this material. The accretion flow could respond by ejecting a powerful wind, as originally suggested by Shakura & Sunyaev (1973). Such winds could be the origin of AGN feedback, setting the $M_{\rm BH} - \sigma$ relation (King 2003), but the wind losses reduce the mass accretion rate onto the

⋆ E-mail: aya@shibaura-it.ac.jp

© 2019 The Authors

central black hole to around Eddington limit, so this does not solve the problem of black hole growth in the early Universe. Nonetheless, there is an alternative way for the accretion flow to exceed the Eddington limit. The Shakura & Sunyaev (1973) equations assume that the energy released through viscosity is radiated locally, but this is not true close to Eddington limit. The flow becomes very optically thick at high mass accretion rates, and photons produced close to the mid plane do not have time to diffuse vertically through the flow in order to be radiated from the surface before the flow itself has moved radially inwards. This optically thick advective cooling by photon trapping is necessarily important in Shakura-Sunyaev discs around Eddington limit. It results in a flow which is moderately geometrically thick, with $H/R \sim 1$ where H is the scale height and R is radius (Abramowicz et al. 1988, slim discs). The radiation escaping from the surface of the flow is limited to the local Eddington flux, but all the additional super-Eddington radiation flux and super-Eddington mass accretion rate is accreted, fueling maximum growth of the black hole. Winds could co-exist with advective flows (e.g. Poutanen et al. 2007), but are not required. Numerical simulations do show both occurring in super-Eddington flows but the ratio of power between these two processes is not clear (e.g. Kitaki et al. 2018 and references therein). However, both advection and winds have rather similar effects on the emitted spectrum, as they both lead to the emitted flux being limited to the local Eddington flux. We thus consider advective cooling alone, and use the data to guide our thinking.

It is clear that AGN spectra in general are more complex than expected from simple blackbody disc models. This makes them different to the stellar mass black hole binaries, where the spectra can often be well fit by an optically thick disc component, though even the most disc dominated spectra show a small tail of emission to higher energies (Remillard & McClintock 2006; Done, Gierliński, & Kubota 2007). However, in AGN, there are no spectra which are as disc dominated as those seen in the black hole binaries. The optical/near UV generally does look blue enough to be the outer disc, especially when dust corrections are taken into account (e.g. Davis, Woo, & Blaes 2007; Baron et al. 2016), but the soft X-rays appear to be dominated by an optically thick, warm Comptonised component of $kT_e \sim 0.2 \sim 1$ keV, while the higher energy X-ray emission requires an additional much hotter, optically thin region (e.g. Elvis et al. 1994). While the origin of these components are not understood, they are surely powered ultimately by gravitational energy released by the accreting matter. Since there is something that looks like an outer disc in the optical/near UV then we can use this to measure the mass accretion rate powering this emission. The disc equations assume that mass accretion rate is constant with radius, so having measured its value in the outer disc sets the luminosity of the disc at all radii via the Novikov-Thorne (NT) emissivity (Novikov & Thorne 1973).

The observed spectral complexity can be parameterised by a radial stratification of the flow. Thermalisation is more or less complete in the outer disc, giving blackbody emission, but inwards of some radius the flow heating concentrates towards the upper layers, making a sandwich geometry which hardwires the soft X-ray excess spectral index to that observed (Petrucci et al. 2018). Then at some smaller radius the flow evaporates completely, making the hard X-ray coronal region (the AGNSED model in XSPEC by Kubota & Done 2018 (hereafter KD18), an upgrade of the original OPTXAGNF model of Done et al. 2012). This approach effectively combines a physically based emissivity prescription which sets the overall energetics, with enough free parameters to fit the data.

However, these models cannot fit to super-Eddington flows, as the advection/wind losses from the inner disc reduce its emitted luminosity compared to that required to power the outer disc. Again, this is most clearly seen in the extreme Narrow Line Seyfert 1 AGN, where the mass accretion rate required to fit the observed (very disc like) optical/UV continuum predicts far too much luminosity at higher energies for any reasonable black hole mass (Jin, Done, & Ward 2016; Done & Jin 2016; Jin et al. 2017) The alternative is to fit with slim disc models, but while super-Eddington sources are actually the most disc like of all AGN (see e.g. Pounds, Done, & Osborne 1995; Jin et al. 2012; Done et al. 2012), they still show the warm and hot Comptonisation regions which make them difficult to fit with purely blackbody disc emission models (Mineshige et al. 2000; Puchnarewicz et al. 2001).

Here we extend our previous three-radial zone approach to super Eddington flows, to build the first tractable physical spectral model which can fit the data. We simply replace the NT emissivity (which is only appropriate for sub-Eddington flows) with an emissivity which changes from $L(R) \propto R^{-3}$ to R^{-2} when the local disc flux exceeds the Eddington limit to effectively describe the effects of either advection or winds (or both) in suppressing the luminosity of the inner disc. We show that this can fit the best dataset of a highly super-Eddington AGN, RX J0439.6 − 5311, where previous attempts with OPTXAGNF failed (Jin et al. 2017). Energy loss via advection and/or winds decreases the luminosity from the inner disc relative to that expected from the outer disc, enabling slim disc fits to the data with reasonable black hole masses.

We also demonstrate the utility of the code on much more limited datasets from high redshift quasars. We are able to fit the (rest frame) optical/UV spectrum of PSO J006+39 at $z = 6.6$ (Tang et al. 2019) and confirm that this is most likely a super-Eddington flow. We discuss the role of the flow geometry in making the unusually blue optical/UV spectrum seen from this quasar, but find that an inner funnel would also increase the apparent luminosity from geometric beaming. This reduces the intrinsic mass accretion rate to below Eddington limit, in conflict with the assumption that the inner flow forms a funnel due to super-Eddington mass accretion. More data for this quasar, especially including its X-ray emission, are needed in order to understand the origin of its unusual properties.

2 OVERALL EMISSIVITY OF THE DISC MODEL

The Eddington limit is straightforward to define in stars, as they are spherical. The radially outwards radiation force is balanced by the radially inward gravity. The disc geometry is much less straightforward. Sub-Eddington (thin) discs extend down to the innermost stable circular orbit,

$R_{\rm isco}$, have the radial component of gravity balanced mainly by rotation, while the vertical component $GM/R^2(H/R)$ is balanced by total pressure (gas plus radiation) setting the scale height, H, of the disc. As $L \rightarrow L_{\rm Edd}$ there are multiple other terms which become important e.g. radial pressure terms become important, and $H \rightarrow R$ so rotation is sub-Keplarian. Radial advection of heat becomes important, so not all the energy released is radiated locally, and the inner edge of the flow is not necessarily set by $R_{\rm isco}$ (Abramowicz et al. 1988; Watarai et al. 2000; Heinzeller & Duschl 2007; Abolmasov & Chashkina 2015). Nontheless, we can get use the thin disc equations to gain some physical insight into the results of more detailed numerical studies (see also Abramowicz 2005 for an insightful review).

The overall emissivity for a sub-Eddington disc is given by NT as

$$F_{\rm NT} = \frac{3GM\dot{M}f(r,a^*)}{8\pi R^3} = \frac{L}{4\pi R^2}\frac{3f(r,a^*)}{2\eta(a^*)r}$$

where $f(r,a^*)$ is the relativistic (NT) version of the stress-free inner boundary condition, which depends only on dimensionless radius $r = R/R_g$ ($R_g = GM/c^2$), and spin, a^*, and $f \rightarrow 1$ as $r \rightarrow \infty$. The total luminosity integrated over the entire disc is $L = \eta(a^*)\dot{M}c^2$ where efficiency $\eta(a^*)$, and we use the efficiency factor to define $\dot{m} = \dot{M}/\dot{M}_{\rm Edd}$ where $\dot{M}_{\rm Edd} = L_{\rm Edd}/(\eta c^2)$. Hence $L/L_{\rm Edd}$ is equal to $\dot{m}$ for sub-Eddington discs of any spin.

We can define a local Eddington flux limit assuming a spherically symmetric, static geometry of $F_{\rm Edd}(R) = L_{\rm Edd}/(4\pi R^2)$. The local disc flux reaches this value for $F_{\rm NT}(R) = F_{\rm Edd}(R)$, i.e. at

$$\frac{L}{L_{\rm Edd}} = \dot{m} = \frac{2\eta(a^*)r}{3f(r,a^*)}$$

Here, we first discuss the case for a non-rotating black hole. Figure 1 shows the NT flux for $\dot{m}_{\rm crit}$ (red), compared to the local Eddington flux (black). The flux first touches the local Eddington limit close to the peak of the disc emissivity, at $r = 17.5$ at a critical mass accretion rate of $\dot{m} = \dot{m}_{\rm crit} = 2.39$. At this radius, the curvature is dominated by the stress-free inner boundary condition which keeps the slope almost parallel to the R^{-2} Eddington flux curve rather than being dominated by the large radius behaviour of $F_{\rm NT} \propto R^{-3}$. This simplistic derivation of the critical mass accretion rate is (surprisingly) the same as $\dot{m}_{\rm crit} = 2 \sim 3$ identified by Fig. 3 of Watarai et al. (2000) and Fig. 4.11 of Sądowski (2011), on the basis of more detailed calculations which include the full two dimensional disc structure including rotation and pressure terms.

For $\dot{m} > \dot{m}_{\rm crit}$, the local emissivity of the inner disc becomes less effective than that of NT, as it is limited to the local Eddington flux. The blue line on Fig. 1 shows the result of this simplistic expectation for $\dot{m} = 10$. The radius at which the flux first reaches the local Eddington limit is now much larger, at $r \simeq 200$, and the inner disc is less luminous than predicted from the outer disc assuming NT emissivity. Figure 2 shows this critical radius, $r_{\rm crit}$ at which the flux starts to hit $F_{\rm Edd}$ plotted against $\dot{m}$ for $a^* = 0$. For $\dot{m} \gg \dot{m}_{\rm crit}$, the critical radius occurs away from the emissivity peak, so the behaviour asymptotes to the expected linear relation between $r_{\rm crit}$ and $\dot{m}$ predicted by the intersection of the intrinsic dissipation $\propto L/R^3$ and the local Eddington flux $\propto L_{\rm Edd}/R^2$. We find $r_{\rm crit} = 24.5\dot{m}$ for $\dot{m} \gg \dot{m}_{\rm crit}$. This differs only by factors of order unity to those of other calculations e.g. our $r_{\rm crit}$ is 1.5× smaller than that of Fukue (2004), but is 2× larger than that of Shakura & Sunyaev (1973). There is a much faster increase in $r_{\rm crit}$ with $\dot{m}$ close to $\dot{m}_{\rm crit}$ due to the almost parallel slope of the Eddington flux and emissivity (see Fig. 1)

Advection also changes the structure of the very inner disc, close to the innermost stable circular orbit. Figure 1 also shows that the flux at $\dot{m} = 10$ drops below the local Eddington limit for $r < r_{\rm bc}(= 7.3)$ due to the stress free inner boundary condition. At this point we might expect that we return again to $F_{\rm NT}$ but more detailed models of super-Eddington discs show that both the inner boundary and the emissivity at small radii change systematically above $\dot{m}_{\rm crit}$. We chose to base our model on $\dot{m} - L$ plots of Watarai et al. (2000) and Sądowski (2011). We find that we obtain consistent $\dot{m} - L$ with their plots for both spin 0 and 0.9 when the inner radius $r_{\rm in}$ decreases from $r_{\rm isco}$ to $r_{\rm h}$ (the horizon) above $\dot{m} = 6$ as:

$$r_{\rm in} = \begin{cases} r_{\rm isco} & (\dot{m} \le 6) \\ r_{\rm isco} \cdot \left(\frac{\dot{m}}{6}\right)^{\log(\frac{r_{\rm h}}{r_{\rm isco}})/\log(\frac{100}{6})} & (6 < \dot{m} \le 100) \\ r_{\rm h} & (100 < \dot{m}) \end{cases} \quad (1)$$

This increases the very inner disc emissivity, so there is more flux emitted than predicted by $F_{\rm NT}$ in this region where the NT disc has its emission strongly suppressed by the stress-free inner boundary condition. We again base our approach to approximately match to Watarai et al. (2000) for spin 0, and Sądowski (2011) for spin 0 and 0.9. We define the inner radius at which the flux drops below the local Eddington flux due to the boundary condition as $r_{\rm bc}$. Then for $\dot{m} > \dot{m}_{\rm crit}$ we define the emissivity at $r_{\rm in} < r < r_{\rm bc}$ as:

$$F_{\rm slim} = \begin{cases} F_{\rm NT}\left(\frac{\dot{m}}{\dot{m}_{\rm crit}}\right)^{\log(\frac{F_{\rm Edd}}{F_{\rm NT}})/\log(\frac{6}{\dot{m}_{\rm crit}})} & \dot{m}_{\rm crit} < \dot{m} < 6 \\ F_{\rm Edd} & \dot{m} \ge 6 \end{cases} \quad (2)$$

This sets the local flux at all radii as a smoothly varying function with $F_{\rm slim} \le F_{\rm Edd}$, giving a local effective blackbody temperature of $\sigma T_{\rm eff}^4 = F_{\rm slim}$. All these approximations to the local emissivity are included in Fig. 3a, where we calculate the flux for a $10^7 M_\odot$ black hole with $a^* = 0$. Advection makes the emissivity profile flatter than that of NT disc, and the emissivity changes smoothly in the inner region for $\dot{m} = \dot{m}_{\rm crit} = 2.39 \rightarrow 6$, as $r_{\rm in}$ decreases from $r_{\rm isco} \rightarrow r_h$ (i.e. $6 \rightarrow 2$ for spin 0) for $\dot{m} = 6 \rightarrow 100$. Figure 3b shows the corresponding fluxes for $a^* = 0.9$. There is now much less difference in inner disc radius, as $r_{\rm isco} = 2.3$ and $r_{\rm h} = 1.3$.

Figure 4 shows the resulting spectra, again for $a^* = 0$ (panel a) and $a^* = 0.9$ (panel b). We integrate each spectral model to derive a bolometric luminosity as a function of $\dot{m}$. Figure 5 shows these for $a^* = 0$ compared to the more detailed calculations by Watarai et al. (2000) and Sądowski (2011). Their data (taken from Fig. 3 in Watarai et al. (2000) and Fig. 4.11 in Sądowski (2011) using GraphClick[1]) are rescaled from their definition of mass accretion rate onto our $\dot{m}$.

[1] http://www.arizona-software.ch/graphclick

It is clear that our model reproduces the overall bolometric luminosity within the uncertainties of previous calculations, and in particular is closest to the best current calculations for spin 0 (Watarai et al. 2000; Sądowski 2011). Watarai et al. (2000) do not include spin, so we only use Sądowski (2011) to compare with our spin 0.9 results. Figure 6 shows our model $L/L_{\rm Edd}$ versus $\dot{M}c^2/L_{\rm Edd}$ as used by Sądowski (2011). Rather surprisingly, our models for $a^* = 0.9$ show slightly less emissivity at sub-Eddington rates than Sądowski (2011). This is because they do not set $r_{\rm in} = r_{\rm isco}$ for sub-Eddington rates. Instead, they use the (viscosity dependent) radius where the effective potential forms a self crossing Roche lobe (potential spout). For spin of 0.9 this gives $r_{\rm in} = 1.96$, smaller than $r_{\rm isco} = 2.32$, (hence efficiency of ~ 0.19 rather than 0.15) for $\dot{m} > 0.3$ (Abramowicz et al. 2010). Given that this radius is dependent on viscosity, and the emission from these inner radii will be strongly affected by gravitational redshifts and the unknown disc geometry, we choose to keep $r_{\rm in} = r_{\rm isco}$ below $\dot{m} = 6$, as in equation 1.

In summary, advection changes the structure of the inner disc for $r \leq r_{\rm crit}$. It decreases the inner disc emissivity from $r_{\rm bc} < r < r_{\rm crit}$, but increases it slightly in the very innermost region, $r_{\rm in} < r < r_{\rm bc}$. The decrease is always more important, so the inner region of the slim disc is always less luminous than predicted by NT emissivity. This removes a key spin diagnostic from energetics. Done et al. (2013) show how the observed outer disc optical/UV emission determines the mass accretion rate, and so predicts the inner disc luminosity modulo black hole spin. Higher spin gives a smaller inner disc radius, so more emissivity, so the observed inner disc emission can be used to determine black hole spin. Some extreme AGN have inner discs which are underluminous even for zero spin assuming NT emissivity, so these strongly constrain spin to be low (Done & Jin 2016; Jin, Done, & Ward 2016; Jin et al. 2017). However, these AGN are most probably super-Eddington, where the inner disc emissivity is strongly reduced, which removes the constraint on low black hole spin.

Advection also removes the other black hole spin diagnostic, namely the position of the inner disc edge as seen via relativistic smearing of the iron line. The disc inner edge is now set by pressure forces as well as gravity, and can be inwards of the innermost stable circular orbit. Thus a very broad iron line, implying a very small inner radius, does not necessarily imply high spin for a super-Eddington flow.

3 SPECTRAL MODEL

The sub-Eddington accretion flow model AGNSED (KD18) is able to reproduce the broadband SED of most AGN and quasars assuming the NT emissivity for a given $\dot{M}$ throughout the disc. Unlike 'pure' disc models, which assume that the dissipated power is emitted as blackbody at all radii, it splits the disc into three different emission regions as schematically shown in Fig. 7. The luminosity in the inner region, from $R_{\rm in}$ and $R_{\rm hot}$, is dissipated in hot material, forming a Comptonised spectrum extending up to high energies, while that from $R_{\rm hot}$ to $R_{\rm warm}$, is emitted instead in an optically thick, warm Comptonising region, and only the outer regions, from $R_{\rm warm}$ to $R_{\rm out}$, completely thermalise and emit as a standard blackbody.

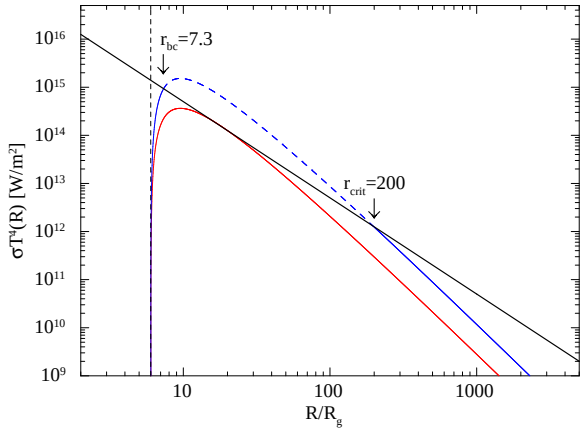


Figure 1. Emissivity is plotted against r fir a 10^7 $M_\odot$ black hole. $F_{\rm NT}$ for $a^* = 0$ of $\dot{m} = 2.39$ and 10 are shown with red solid line and blue solid (or dashed) line, respectively. $F_{\rm Edd}$ is shown with black solid line. $r_{\rm isco}$ is indicated with a vertical dashed line.

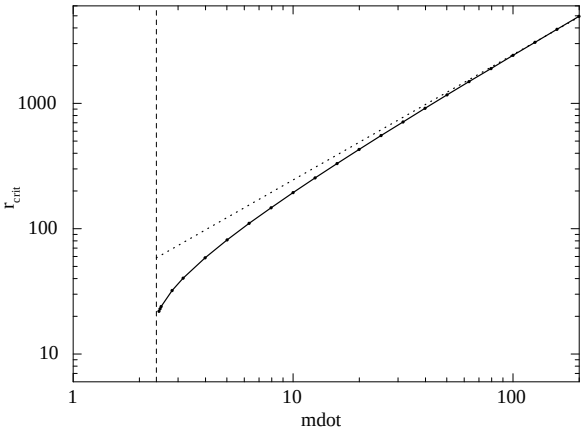


Figure 2. The calculated critical radius $r_{\rm crit}$ is plotted against $\dot{m}$. Solid line indicates the result by $4\pi\sigma R_{\rm crit}^2 T(R_{\rm crit})^4 = L_{\rm Edd}$, Dotted line represents $r_{\rm crit} = 24.5\dot{m}$. The dashed vertical line indicates $\dot{m} = 2.39$.

We follow this general model, but replace the NT emissivity with the slim disc emissivity detailed above. Though the slim disc is expected to give larger H/R, it is complicated to include this geometrical effects to the model. We thus still employ the thin disc geometry as is done for AGNSED. One key difference is that the AGNSED model assumes that the hot inner flow region does not have an underlying disc component. This is because the lowest luminosity AGN have hard X-ray spectra with photon index $\Gamma < 1.9$. Reprocessing of the coronal X-rays in any underlying cool disc material provides seed photons for the hot Comptonisation and sets $\Gamma = 1.9$ as a lower limit for the spectral index even with a non-emitting 'passive' disc. While the higher luminosity AGN typically have X-ray spectra which are softer than this limit, the observed spectral indices are remarkably well predicted for $0.03 < L/L_{\rm Edd} < 1$ assuming this truncated disc geometry. However, for super-Eddington flows it seems very unlikely that this continues (see Section 2) so we consider a slab corona for the hard X-rays at these high mass accretion rates instead truncated disc with spherical hot flow.

Another, more minor difference from AGNSED is that

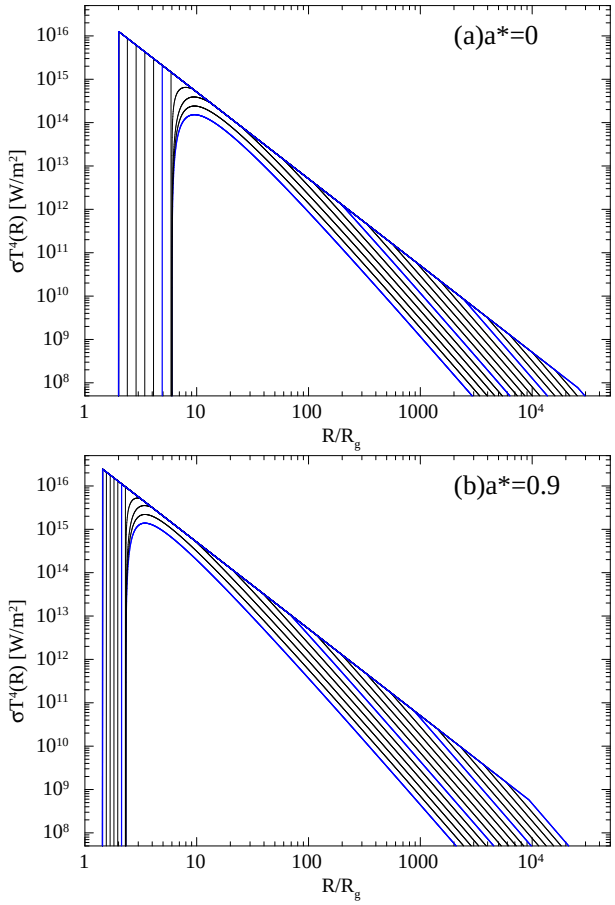


Figure 3. The local flux, $F(R) = \sigma T_{\rm eff}(R)^4$ is plotted against radius r for a black hole of $M = 10^7 M_\odot$ with different $\dot{m}$; from $\log \dot{m} = 0$ to 3 with $\Delta \log \dot{m} = 0.2$. Thick blue solid lines represent $\log \dot{m} = 0$, 1, 2 and 3. Black hole spin is set to be $a^* = 0$ (panel a) and 0.9 (panel b).

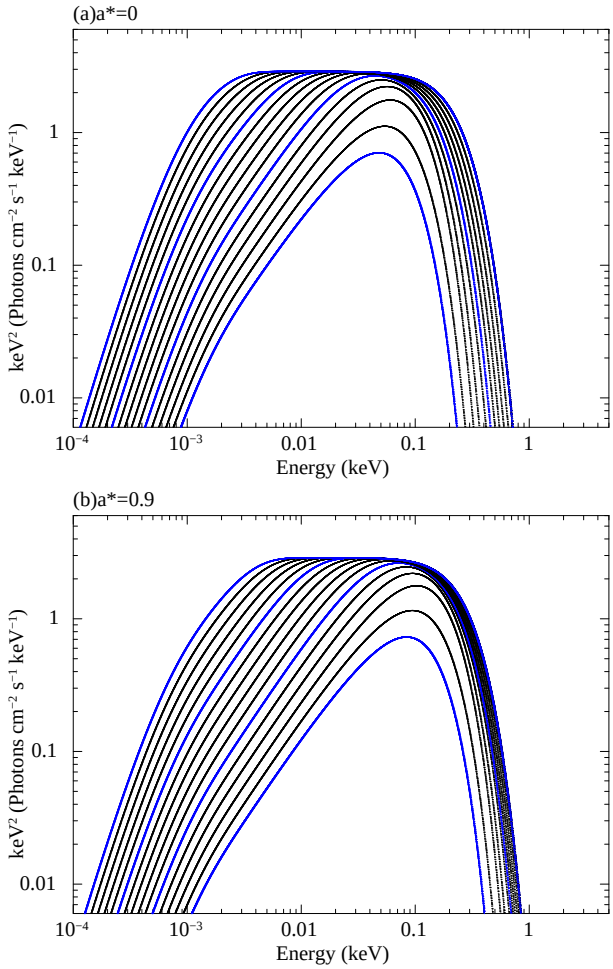


Figure 4. The emergent spectra for a 10^7 $M_\odot$ black hole with different $\dot{m}$ from $\log \dot{m} = 0$ to 3 with $\Delta \log \dot{m} = 0.2$. Distance and inclination are set to be 100 Mpc and 0°, respectively. Colours are the same as Fig. 3

we do not include the contribution of reprocessed hard X-ray flux, as we expect that the inner disc will puff up to some extent (see section 5), so that there is self-occultation preventing illumination of the outer disc. Even without this effect, the contribution from reprocessing is small for high Eddington ratio AGN as they typical have $L_{\rm X}/L_{\rm bol} \ll 1$ (see Fig.3 in KD18).

We name this new model AGNSLIM. We show a comparison of AGNSLIM (coloured lines) versus AGNSED (grey) in Fig. 8 for $\dot{m} = 1$, 3, 10, 30 and 100. The dot-dashed lines show the pure intrinsic blackbody emission without any Comptonisation, while the solid lines show the resulting spectra for a set of fiducial parameters which are characteristic of high $\dot{m}$ AGN ($\Gamma_{\rm warm} = 2.7$, $kT_{e,\rm warm} = 0.2$ keV, $r_{\rm warm} = 20$, $\Gamma_{\rm hot} = 2.4$, $kT_{e,\rm hot} = 100$ keV and $r_{\rm hot} = 10$ for a $10^7 M_\odot$ black hole with spin 0 viewed at 0° inclination). There is no visible difference between AGNSED and AGNSLIM at $\dot{m} = 1$ (red) as this is below $\dot{m}_{\rm crit} = 2.39$, so the local flux is set by the standard NT emissivity and never hits the saturation point at the local Eddington limit. The different geometry for the hot X-ray regions (disc corona rather than truncated disc) does make a difference to the high energy X-ray flux, but the two are equal for the face on inclination assumed here. There is a slight difference at $\dot{m} = 3$ (green) as this just

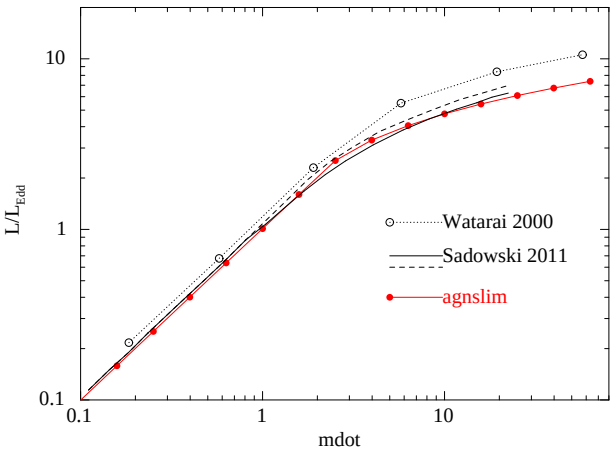


Figure 5. Eddington ratio as a function of $\dot{m}$ based on AGNSLIM for spin 0. Data points of AGNSLIM and Fig.3 of Watarai et al. (2000) are shown with filled red circles and open black circles, respectively. A solid line and a dashed line is theoretical prediction by Sądowski (2011) in Fig. 4.11, with $\alpha = 0.01$ and 0.1.

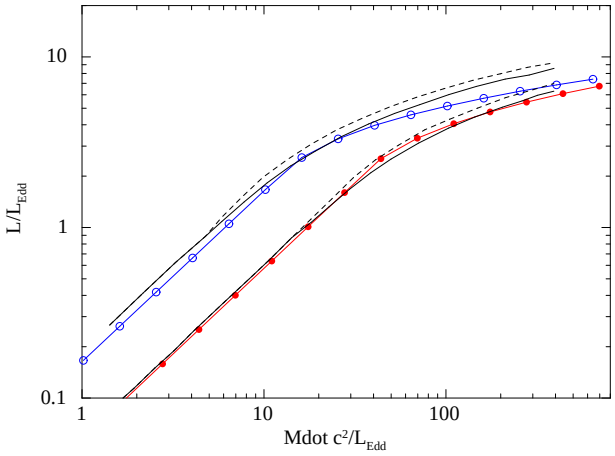


Figure 6. Eddington ratio as a function of $\dot{M}c^2/L_{\rm Edd}$ based on AGNSLIM. Same as Fig. 5, solid lines and dashed lines are theoretical predictions by Sądowski (2011) in Fig. 4.11, with $\alpha = 0.01$ and 0.1. Case of black hole spin of $a^* = 0$ and 0.9 are shown with red filled circles and blue open circles, respectively.

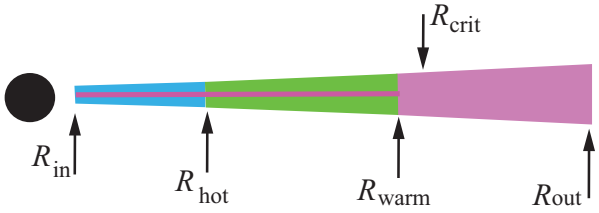


Figure 7. Geometry

touches the local Eddington limit, so has flux saturated at this limit from $r = 35 \rightarrow 7$. This produces a noticeable drop in the hottest blackbody disc emission ($r = 35 \rightarrow 20$) and in the warm Comptonisation emission from $r = 20 \rightarrow 10$. However, the hot Comptonisation in AGNSLIM is slightly brighter than that in AGNSED due to the enhanced emissivity from $r_{\rm in} \rightarrow r_{\rm bc}$. The hottest part of the blackbody disc continues to decrease relative to AGNSED as $\dot{m}$ increases from 10 (blue) to 30 (cyan) and finally to 100 (magenta). This saturation starts to become evident in the UV for $\dot{m} > 10$, and even extends into the optical for $\dot{m} > 100$ for this black hole mass. Similarly, the warm Comptonisation emission continues to decrease relative to AGNSED to an almost constant flux in AGNSLIM as the region from $r = 10 \rightarrow 20$ is all saturated to the local Eddington flux. However the hot Compton component shows more complex behaviour as the increase in emissivity from $r_{\rm bc} \rightarrow r_{\rm in}$ relative to NT can offset some of the decrease from $r = 10 \rightarrow r_{\rm bc}$.

4 APPLICATION TO THE OBSERVED SED OF RX J0439.6-5311

RX J0439.6 – 5311 is a type I Narrow Line quasar which has the smallest Hβ full-width-at-half-maximum (FWHM) of 700 ± 140 km s^{-1} among the 110 soft X-ray selected AGN in Grupe et al. (2004) and Grupe (2004). This, together with the monochromatic luminosity at 5100 Å can be used to estimate mass of 3.9×10^6 $M_\odot$ (using Kaspi et al. 2000). Jin et al. (2017) re-analysed the components in the Hβ line profile and estimate the broad line width of ~ 850 km/s, giving slightly larger mass estimates of 9.4×10^6 $M_\odot$ (Vestergaard & Peterson 2006) or 6.7×10^6 $M_\odot$ (Woo & Urry 2002).

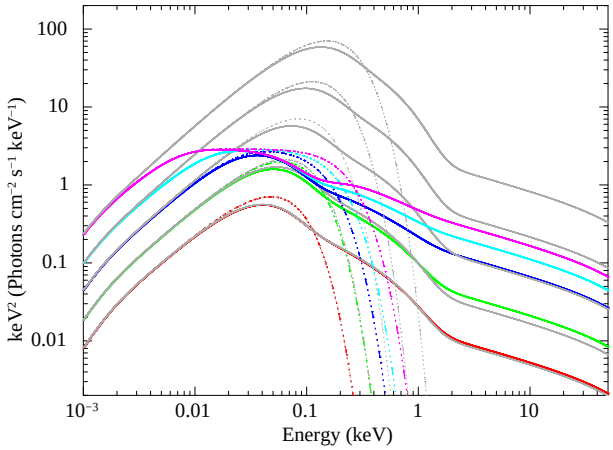


Figure 8. Comparison of AGNSED (gray) and AGNSLIM (colour) for $M = 10^7$ $M_\odot$ black hole with $i = 0°$. $\dot{m} = 1$ (red), 3 (green), 10 (blue), 30 (cyan) and 100 (magenta) are shown with $kT_{e,\rm warm} = 0.2$ keV, $kT_{e,\rm hot} = 100$ keV, $\Gamma_{\rm warm} = 2.7$, $\Gamma_{\rm hot} = 2.4$, $r_{\rm hot} = 10$ and $r_{\rm warm} = 20$. Intrinsic disc emissions without any Comptonisation are shown with dotted lines.

This NLS1 has one of the best broadband datasets of any super-Eddington AGN, with extremely low galactic absorption column of $N_{\rm H} = 7.45 \times 10^{19}$ cm^{-2}, corresponding to reddening $E(B-V) = 1.7 \times 10^{-22} N_{\rm H} = 0.127$. This means that the AGN continuum can be seen up to 912 Å in the rest frame, and above 0.1 keV, with less than an order of magnitude gap in energy coverage from interstellar absorption. We use the optical/UV/X-ray data from Jin et al. (2017), but exclude the IR as this is dominated by reprocessed emission from hot dust rather than by the accretion flow itself.

Jin et al. (2017) fit these data using the OPTXAGNF model, with redshift fixed at $z = 0.242$, i.e. comoving radial distance of 985.0 Mpc and inclination of $i = 30°$, together with Galactic extinction and reddening (TBNEW, with abundances of Wilms, Allen, & McCray (2000) and REDDEN) fixed to the parameters above. They found that the SED could not be well fit with the NT based emissivity for black hole masses below $\sim 2 \times 10^7 M_\odot$. The lower black hole masses from the virial estimates give SED models which strongly over predict the observed soft and hard X-ray luminosity for the mass accretion rates required to fit the optical/UV outer disc continuum.

Here we first explore the optical/UV continuum alone. Figure 8 shows that for extreme $\dot{m}$ the flux saturation at the local Eddington limit starts to affect even the optical/UV emission. The advected flux means that there is less flux emitted so the UV continuum slope becomes significantly redder. This should give a secure upper limit of $\dot{m}$ from the optical/UV data alone, and hence a secure lower limit to the black hole mass.

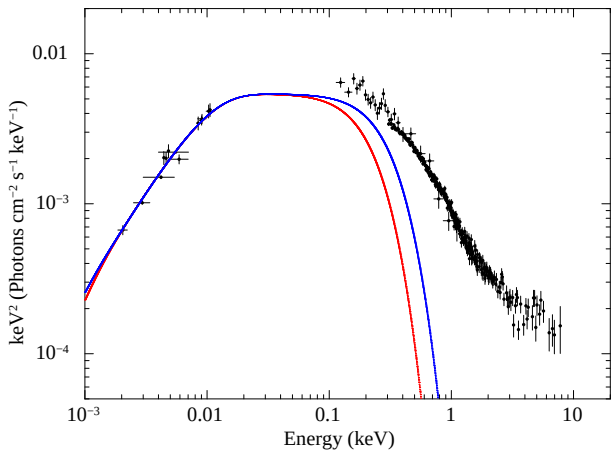


Figure 9. Absorption corrected broadband SED of RX J0439.6−5311 and AGNSLIM of lower limit mass $M = 2.8 \times 10^6\ M_\odot$ without warm/hot Comptonising corona. The SED is deconvolved based on the best fit model in section 4.2. Blackhole spin is assumed to be $a^* = 0$ (red) and 0.9 (blue).

4.1 A secure lower limit for mass from optical/UV data alone

As shown in Fig.4 of Jin et al. (2017), the slope of optical-UV data points in the SED of RX J0439.6−5311 are in good agreement with the standard NT disc. There is no strong deviation (flattening) from the NT disc in the optical/UV range which would be expected if the disc had become super-Eddington at radii which emit in this bandpass (Fig. 4 and 8). Thus lack of such flattening gives us a secure lower limit for M from this upper limit for $\dot{m}$. We use a pure disc model, as it is only the X-rays which require the Comptonised components.

We fix the redshift, distance and galactic absorption column at the same values as Jin et al. (2017), but fix $i = 0°$. We then fit all the optical-UV data without any Comptonisations with the same parameters except normalizations of the (non-simultaneous) HST and ground based optical spectra are multiplied by the best fit factor derived from the broad band SED spectrum (see next section). For a black hole of $a^* = 0$, we find an upper limit on $\dot{m} \simeq 45$, and corresponding lower limit on the mass of $2.8 \times 10^6 M_\odot$. Since we assumed a face on geometry, this can be taken as the secure lower limit for the mass of RX J0439.6−5311. We have same lower limit mass of $2.8 \times 10^6 M_\odot$ with higher $\dot{m}$ of ~ 120 for a black hole of $a^* = 0.9$. This is because the saturated flux does not depend on black hole spin but on black hole mass.

Red line and blue line in Fig. 9 shows the pure disc AGNSLIM model for a black hole of $M = 2.8 \times 10^6\ M_\odot$ with $\dot{m} = 45$ ($a^* = 0$) and $\dot{m} = 120$ ($a^* = 0.9$), respectively. The absorption corrected broad band data are overlaid on this figure, clearly showing that the higher energy spectra cannot be explained by a slim disc model where the emission is blackbody. It is also clear that this minimum mass model for the optical/UV does not have enough luminosity to power the observed emission, so a higher black hole mass/lower mass accretion rate with lower advective losses is required in order to match the data.

4.2 Broadband SED fit

We now fit the entire broadband SED with AGNSLIM model. We again renormalize the optical-UV data to that of XMM-OM data. We first allow the normalisation of the *ROSAT* data to be free relative to the XMM EPIC-pn data over the same bandpass of 0.3–1keV, but the resulting ratio was $1.02^{+0.07}_{-0.08}$, so we fixed this at 1.

The AGNSLIM model with $a^* = 0$ reproduces the broadband SED fairly well, with the best fit χ^2_ν around 1.30 for a range of black hole masses, from $5 \times 10^6\ M_\odot$ to $1.4 \times 10^7\ M_\odot$, corresponding to $\dot{m} \simeq 14$ to 2. The high mass/low mass accretion rate fit is consistent with the fits of Jin et al. (2017), as $\dot{m} = 2 < \dot{m}_{\rm crit}$ so does not reach the local Eddington flux, so still has NT emissivity as assumed in the models used in Jin et al. (2017). However, the AGNSLIM model now allows lower mass solutions. We fix the mass at $8 \times 10^6\ M_\odot$ as derived from the Hβ line profile, and show the best fit parameters in table 1. This model is overlaid on broadband SED in Fig. 10, with the inner hot Comptonising corona (blue), the warm Comptonising corona (green) and outer disc (magenta) shown separately. The resultant accretion rate of $\dot{m} = 5.4$ is in the slim disc regime, and gives an observable luminosity of $\sim 2.5 L_{\rm Edd}$ (see Fig. 5). The inner hot corona region is from $r_{\rm hot} = 9.4$ to $r_{\rm in} = 6$, as $\dot{m} = 5.4$ is not high enough to extend the inner disc below $r_{\rm isco}$ (see equation 1). This gives $L_{\rm hot} = 0.4 L_{\rm Edd}$, which is fairly large compared to some sub-Eddington AGN (KD18). We repeat the fit for spin of $a^* = 0.9$. As shown in table 1, the model can fit the data with similar χ^2 to $a^* = 0$. Again $r_{\rm in} = r_{\rm isco}$ but the high spin means that inner part of the flow now extends considerably closer to the central black hole. Thus the hot inner corona region is more compact, at $r_{\rm hot} = 2.7$ to keep the observed $L_{\rm hot}$ of $\sim 0.4 L_{\rm Edd}$. As a result, the warm compact region is also smaller, with $r_{\rm warm} = 6.1$.

However, in both these fits the soft and hard X-ray emission regions are close enough to the black hole that General Relativistic effects should be important (Cunningham 1975; Zhang et al. 1997). These will be dominated by gravitational and transverse redshift as the face on inclination means that the doppler shift from the orbital velocity is small. The redshifts reduce the observed luminosity, but in a way which is difficult to calculate exactly as slim discs are no longer flat or Keplarian, so the ray tracing depends on the poorly known geometry and dynamics of the flow (Vierdayanti et al. 2013). Even for sub-Eddington, flat discs, these effects are not easy to include as the GR transfer functions available in XSPEC are normalised to unity, rather than incorporating the radially dependent loss of photons down the black hole. Instead, we follow the approximate treatment suggested in Done et al. (2013), using the standard XSPEC transfer function KDBLUR from $r_{\rm in}$ to $r_{\rm hot}$ on the hot component, $r_{\rm hot}$ to $2r_{\rm hot}$ on the warm comptonisation, and $r_{\rm warm}$ to $2r_{\rm warm}$ on the outer disc. This at least gives some indication of the size of the uncertainties introduced by GR effects (see also Porquet et al. 2019). We show results for $a^* = 0$ and 0.9 in table 1. The best fit for $a^* = 0$ and black hole of mass $8 \times 10^6\ M_\odot$ is now considerably worse than before, at $\chi^2/dof = 948/711$. This is because the GR effects reduce both the soft and hard X-ray flux. The mass and spin are fixed in this fit, and $\dot{m}$ is tightly constrained by the optical/UV data, and even increasing $r_{\rm hot}$ and $r_{\rm warm}$ does

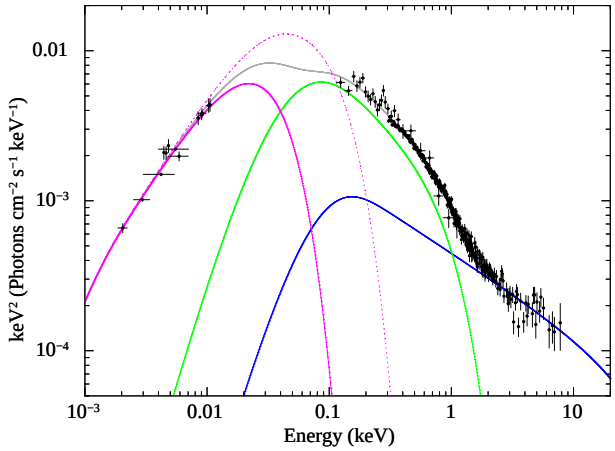


Figure 10. Same as Fig. 9 but with the best fit AGNSLIM model without GR for a black hole mass 8×10^6 $M_\odot$ and $a^* = 0$ (grey), showing the outer blackbody disc (magenta), warm comptonised disc-corona (green) and hot inner disc-corona (blue). The dashed magenta line shows the same slim disc model but with pure blackbody emission at all radii.

not give enough X-ray flux. Allowing the black hole mass to be free does allow us to recover a fit including GR of comparable quality to one without, but requires a mass of $> 10^7$ $M_\odot$, and hence $\dot{m} < \dot{m}_{\rm crit}$ out of the slim disc regime. There are similar issues with including GR at higher spin, but the stronger suppression of the soft and hard X-ray flux is less of a problem as $r_{\rm hot}$ and $r_{\rm warm}$ were so small without GR that they can increase enough to compensate for the redshift losses.

5 APPLICATION TO $Z = 6.621$ QUASAR PSO J006 + 39

High mass accretion rates are expected in the gas rich early Universe, but so far there is only one AGN known at $z > 6$ which is strongly super-Eddington. This is the recently discovered quasar PSO J006 + 39, at $z = 6.621$ (Tang et al. 2017), with a black hole mass measured from the width of the Mg_{II} line of $(1.4–1.7) \times 10^8$ $M_\odot$ (Tang et al. 2019). This paper also showed that the rest frame optical/UV continuum was extremely blue, with $\alpha_\nu = 0.94$ (i.e, photon index $\Gamma = 0.06$), significantly bluer than the slope of the standard disc of $\alpha_\nu = 1/3$ (i.e., $\Gamma = 2/3$), and significantly bluer than the majority of quasars at either high z (Tang et al. 2019 and references therein) or more locally (Xie et al. 2016). A slope which is redder than the standard disc is easy to obtain (dust reddening in the host galaxy: Baron et al. 2016, Davis et al. 2007 ; or a colour temperature correction onset in the UV: Done et al. 2012, or advection losses, see sections 3 and 4). However, a bluer slope is more difficult to explain. Tang et al. (2019) showed that this could be obtained if the disc is significantly smaller than expected from the self gravity radius of $r_{\rm out} \sim 5000$. They fit PSO J006+39 using a model where the outer edge of the accretion disc is at $r_{\rm out} \sim 230$, with a highly super-Eddington rate of $\dot{m} \sim 9$.

These fits were derived using the OPTXAGNF model in XSPEC, which is similar to AGNSED in assuming NT emissivity. Yet this is not self consistent as at such high $\dot{m}$ optically thick advection must be important. We thus fit the optical/UV continuum spectrum with our AGNSLIM model. We use the data from Tang et al. (2019) which is corrected for redshift and for Galactic absorption, and fix the black hole mass at 1.6×10^8 $M_\odot$. Since the data have been redshift corrected we use the luminosity distance fixed at 66.1 Gpc to derive flux. We assume a pure blackbody disc model since there are (currently) no published X-ray data from which to determine the hot coronal component. We neglect GR as the (rest frame) optical/UV data are not from the inner disc where these effects become important.

5.1 AGNSLIM model fits

We first fit the data by setting $r_{\rm out}$ to the value determined by the self-gravity and we fix $\cos i = 1$. We confirm that this gives a very poor fit, with $\chi^2/dof = 171/19$ and $123/19$ for $a^* = 0$ and 0.9, respectively, showing that the data are much bluer than the model, as before. We then follow Tang et al. (2019) and allow $r_{\rm out}$ to be a free parameter. The results are shown in table 2 and Fig. 11. The spectrum is well reproduced by the model with $\dot{m} = 2.2$ and $r_{\rm out} = 140$ for spin 0, and for $\dot{m} = 4.4$ and $r_{\rm out} = 145$ for spin 0.9. These values of $r_{\rm out}$ are consistent with the result of Tang et al. (2019) as the difference between NT based emissivities and the slim disc emissivity is not large in this regime. Thus our fits confirm the requirement for an extremely small disc outer radius in this super-Eddington object.

Geometrical effects may give a solution for this difference in outer radius, as proposed by Tang et al. (2019). The inner slim disc region should be puffed up in highly accreting black holes (see Fig. 12). Viewing angles which intersect the opening angle of the inner disc will have the emission from $r_{\rm in} \rightarrow r_{\rm crit}$ geometrically boosted by a factor $\sim (1 - \sin\theta_H)^{-1}$ where $\tan\theta_H = H/R$. Thus it may appear that the disc itself ends at $r_{\rm crit}$ as this geometric beaming makes the inner disc emission brighter than that of the outer disc beyond $r_{\rm crit}$. This is an initially very attractive solution as the values of $r_{\rm out}$ determined above are very similar to the values of $r_{\rm crit}$ expected for these mass accretion rates.

However, any geometric beaming reduces the required mass accretion rate. The radii emitting the optical/UV flux is still mostly in the standard NT regime so gives flux $\propto (M\dot{M})^{2/3} \propto (M^2\dot{m})^{2/3}$. Hence enhancing the flux within the funnel by a factor b will decrease $\dot{m}$ by a factor $b^{3/2}$. Thus, large beaming factors mean that the underlying flow here would not be super-Eddington, in conflict with the assumption that the super-Eddington flux has caused the disc to puff up. However slim discs probably do not form extreme funnels, they have $H \lesssim R$ for $\dot{m} \gg 1$ (Abramowicz et al. 1988; Lasota et al. 2016). Thus these should be only mildly beamed by less than a factor of 3-4 (see also Atapin, Fabrika & Caballero-García 2019), although any wind may enhance the funnel geometry beyond this (e.g., Abolmasov et al. 2009; Poutanen et al. 2007). The unbeamed AGNSLIM fits required $\dot{m} = 2 \rightarrow 4$ for $a^* = 0 \rightarrow 0.9$ so, AGNSLIM even with mild beaming with $b = 3$ (i.e. fixing the normalisation to this value) means that $\dot{m}$ is reduced to below Eddington, in conflict with the model where the disc puffs up due to a strongly super-Eddington mass accretion rate. Thus our conclusion is that it is difficult to explain the observed very blue continuum in PSO J006 + 39 by emission

Table 1. The best fit parameters of RXJ 0439.6 – 5311.

		$a^*=0$ without GR	$a^*=0.9$ without GR	$a^*=0$ with GR†	$a^*=0.9$ with GR†
$\dot{m}$		$5.43^{+0.12}_{-0.11}$	13.7 ± 0.3	$5.61^{+0.14}_{-0.11}$	$13.1^{+0.5}_{-0.2}$
$\Gamma_{\rm hot}$		2.53 ± 0.07	2.55 ± 0.07	$2.60^{+0.04}_{-0.06}$	$2.49^{+0.05}_{-0.07}$
$\Gamma_{\rm warm}$		$2.69^{+0.04}_{-0.05}$	2.67 ± 0.07	2.58 ± 0.03	$2.67^{+0.04}_{-0.02}$
$kT_{e,\rm warm}$	keV	$0.252^{+0.013}_{-0.012}$	$0.247^{+0.016}_{-0.014}$	$0.253^{+0.011}_{-0.006}$	$0.330^{+0.021}_{-0.013}$
$r_{\rm hot}$		$9.4^{+0.7}_{-0.5}$	$2.71^{+0.09}_{-0.19}$	$12.0^{+1.0}_{-0.9}$	4.2 ± 0.3
$r_{\rm warm}$		60^{+9}_{-7}	$6.11^{+0.11}_{-0.21}$	100^{+3}_{-1}	53^{+14}_{-8}
The other size scales calculated based on the best fit model					
$r_{\rm in}$		6.0	2.0	6.0	2.0
$r_{\rm crit}$		91	100	94	95
$r_{\rm out}$	$\times 10^3$	8.0	12.1	8.1	11.9
χ^2/dof		922.2/711	924.6/711	948.0/711	926.9/711

Electron temperature of the hot comptonising corona is fixed at 20 keV.
Black hole mass is fixed at $8.0 \times 10^6\ M_\odot$.
† General relativistic effects are approximated by KDBLUR with power index of 3. The model is described as KDBLUR(H)*AGNSLIM(HOT COMPTON)+KDBLUR(W)*AGNSLIM(WARM COMPTON)+KDBLUR(O)*AGNSLIM(OUTER DISC).
$r_{\rm in}$ of KDBLUR(H) is fixed at 2 and 6 for $a^*=0$ and 0.9, respectively, and $r_{\rm out}$ of KDBUR(H) is fixed at $r_{\rm hot}$.
$r_{\rm in}$ and $r_{\rm out}$ of KDBLUR(W) are fixed at $r_{\rm hot}$ and $2r_{\rm hot}$, respectively.
$r_{\rm in}$ and $r_{\rm out}$ of KDBLUR(O) are fixed at $r_{\rm warm}$ and $2r_{\rm warm}$, respectively.

dominated by the inner funnel of a super-Eddington flow. Stronger geometric beaming will reduce the intrinsic $\dot{m}$ still further, making an even larger discrepancy between $r_{\rm out}$ as required from fitting the data, and $r_{\rm crit}$ inferred from $\dot{m}$.

The failure of the previous models to give a fully self consistent picture motivates us to consider a more subtle effect of the geometry shown in Fig. 12. The far side of the puffed up disc will be enhanced relative to the outer standard disc as it makes a smaller angle to the line of sight (Kawashima T. in private communication; see also Wang et al. 2014 for similar geometric effects on the illumination of the BLR by a super-Eddington flow). We fix the inclination to 60° to approximate spherical geometry for far side of the puffed up disc, and fit the data for both $a^*=0$ and 0.9. The results are again shown in table 2 and Fig. 11. These again give small outer disc radii of $\sim 190R_g$, This value is almost consistent with $R_{\rm cri}$ for $\dot{m} \sim 10$ ($a^*=0$) or for $\dot{m} \sim 20$ ($a^*=0.9$). Yet here to enhance the edge of puffed flow than the redder outer standard disc by this geometrical effect, extremely high inclination angle of $i = 80° \sim 90°$ is required. Thus it seems unlikely that the far side of the puffed up flow would be able to outshine the redder outer disc emission, so the blue continuum is difficult to explain. Also it seems much more likely that any object we see at such high redshift is the brightest in its class.

We conclude that the most likely solution for the extremely blue continuum in PSO J006 + 39 is that the outer disc is intrinsically small (see also Collinson et al. 2017 for inferred small size outer discs in quasars at $z \sim 1-2$). Alternatively, we could be looking not at a disc at all, but at a wind photosphere which gives approximately blackbody emission.

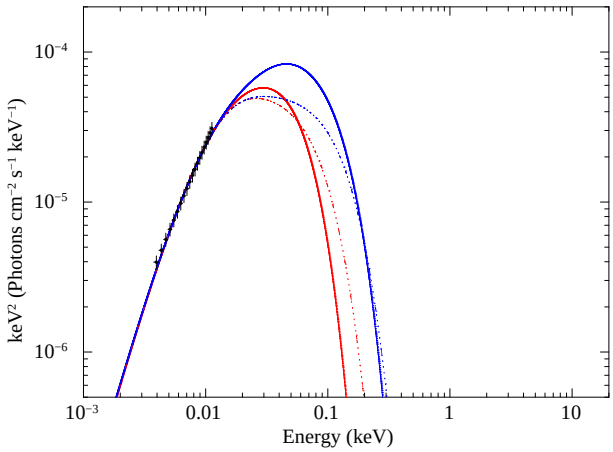


Figure 11. The best fit AGNSLIM model overlaid on the redshift corrected NIR spectrum of PSO J006 + 39. Solid lines and dotted lines correspond to $i = 0°$ and 60°, respectively. Spin parameter a^* is assumed to be 0 (red) and 0.9 (blue) .

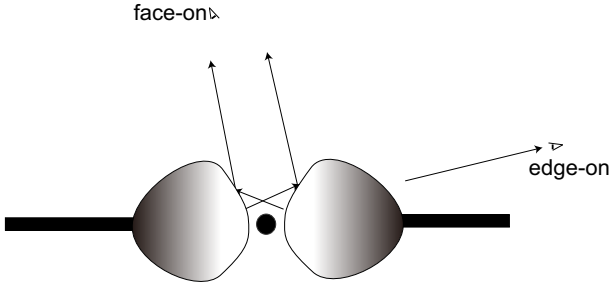


Figure 12. Schematic picture of puffed slim disc.

6 SUMMARY AND CONCLUSIONS

Super-Eddington accretion flows are seen in the local Universe, in some extreme NLS1, ULXs and black hole binary systems, and should be prevalent in the gas rich conditions of the early Universe. Such flows should be less radiatively efficient than standard sub-Eddington discs, as the emitted flux should saturate at the local Eddington limit, with

Table 2. The best fit parameters of PSO J006 + 39.

	$a^* = 0$ ($i = 0°$)	$a^* = 0.9$ ($i = 0°$)	$a^* = 0$ ($i = 60°$)	$a^* = 0.9$ ($i = 60°$)
$\dot{m}$	$2.2^{+0.6}_{-0.3}$	$4.4^{+1.2}_{-0.7}$	12^{+174}_{-7}	$19^{+>1000}_{-7}$
$r_{\rm out}$	140^{+21}_{-19}	145^{+24}_{-21}	189^{+34}_{-23}	194^{+34}_{-27}
The other size scales calculated based on the best fit model				
$r_{\rm in}$	6	2.3	4.6	1.90
$r_{\rm crit}$	—	24	226	148
χ^2/dof	3.90/18	3.45/18	4.46/18	4.38/18

Black hole mass is fixed at $1.6 \times 10^8\ M_\odot$.

the remaining power lost through radial advection and/or winds. We develop a new model for fitting data from super-Eddington flows, AGNSLIM. We base this on the successful sub-Eddington flow model AGNSED (an updated version of OPTXAGNF) which uses the NT emissivity for a constant mass accretion rate, but allows radial stratification of the emission. The outer disc thermalises to a blackbody, and the inner disc dissipates the emission in a hot, optically thin Comptonising region, while intermediate radii are dominated by a warm, optically thick Comptonisation corona. Our new model uses this same radial stratification for the spectrum, but limits the emissivity to the local Eddington flux in order to include the effects of advection and/or winds.

We show that this model can fit the broadband spectrum of RX J0439.6-5311, an extreme NLS1 which could not be fit with a NT emissivity for the most likely black hole masses of $\sim 8 \times 10^6 M_\odot$ as its inner disc is clearly much less luminous than predicted by the high mass accretion rate required to fit the outer disc emission (Jin et al. 2017). Our new model can fit these data with this low black hole mass, implying $\dot{m} = 5 \sim 10$. These slim disc models can no longer constrain black hole spin from the energetics as both low and high spin models have similar emissivity and inner disc radii due to the flux saturation at the local Eddington limit.

Super-Eddington mass accretion rates can solve the problem of the seed black hole mass required for the highest redshift quasars (e.g. Volonteri & Rees 2005). However, most known quasars at $z > 6$ are not super-Eddington. This could be due to evolutionary effects, where they are mostly obscured when accreting at such high rates, so that they only become visible along most sight lines when $\dot{m} \lesssim 1$ (e.g. the review Alexander & Hickox 2012). Nonetheless, there is one strongly super-Eddington quasar at $z > 6.5$, PSO J006+39, which also has an unusually blue rest frame optical/UV continuum (Tang et al. 2019). We fit this with our new model and show that this cannot be easily explained even including geometrical effects which might be expected in the super-Eddington regime. We conclude that these data require that the disc is intrinsically small rather than being puffed up, or that the emission is dominated by a wind photosphere.

The model should also be applicable to the accretion discs in ULXs. Several of these are now known to be pulsars (ULX-P), with neutron star massess strongly requiring highly super-Eddington flows, and the remainder are likely to be black holes with moderately super-Eddington flows (Kaaret, Feng & Roberts 2017; Atapin, Fabrika & Caballero-García 2019). This model will be publically released as part of the XSPEC spectral fitting software.

ACKNOWLEDGEMENTS

We thank to C. Jin and J.-J. Tang for providing us a data set for RX J0439.6 − 5311 in Jin et al. (2017) and PSO J006 + 39 in Tang et al. (2019), respectively. AK acknowledges helpful discussion with S. Mineshige, J. Fukue and T. Kawashima. AK is supported in part from research program in foreign country by Shibaura Institute of Technology. CD acknowledges support from STFC through grant ST/P000541/1. We also thank M. D. Caballero-García as our referee.

REFERENCES

Abolmasov P., Chashkina A., 2015, MNRAS, 454, 3432
Abolmasov, P., Karpov, S., & Kotani, T. 2009, PASJ, 61, 213
Abramowicz, M. A. 2005, Growing Black Holes: Accretion in a Cosmological Context, 257
Abramowicz M. A., Czerny B., Lasota J. P., Szuszkiewicz E., 1988, ApJ, 332, 646
Abramowicz M. A., Jaroszyński M., Kato S., Lasota J.-P., Różańska A., Sądowski A., 2010, A&A, 521, A15
Alexander, D. M., & Hickox, R. C. 2012, New Astron. Rev., 56, 93
Atapin K., Fabrika S., Caballero-García M. D., 2019, MNRAS, 486, 2766
Bañados E., et al., 2018, Natur, 553, 473
Baron D., Stern J., Poznanski D., Netzer H., 2016, ApJ, 832, 8
Boekholt T. C. N., Schleicher D. R. G., Fellhauer M., Klessen R. S., Reinoso B., Stutz A. M., Haemmerlé L., 2018, MNRAS, 476, 366
Collin S., Kawaguchi T., 2004, A&A, 426, 797
Collinson, J. S., Ward, M. J., Landt, H., et al. 2017, MNRAS, 465, 358
Cunningham C. T., 1975, ApJ, 202, 788
Davis S. W., Laor A., 2011, ApJ, 728, 98
Davis S. W., Woo J.-H., Blaes O. M., 2007, ApJ, 668, 682
Done C., Jin C., Middleton M., Ward M., 2013, MNRAS, 434, 1955
Done, C., Davis, S. W., Jin, C., Blaes, O., & Ward, M. 2012, MNRAS, 420, 1848
Done C., Gierliński M., Kubota A., 2007, A&ARv, 15, 1
Done C., Jin C., 2016, MNRAS, 460, 1716
Elvis M., et al., 1994, ApJS, 95, 1
Fukue J., 2004, PASJ, 56, 569
Grupe D., 2004, AJ, 127, 1799

Grupe D., Wills B. J., Leighly K. M., Meusinger H., 2004, AJ, 127, 156
Heinzeller D., Duschl W. J., 2007, MNRAS, 374, 1146
Jin C., Done C., Ward M., Gardner E., 2017, MNRAS, 471, 706
Jin C., Done C., Ward M., 2016, MNRAS, 455, 691
Jin C., Ward M., Done C., Gelbord J., 2012, MNRAS, 420, 1825
Kaaret P., Feng H., Roberts T. P., 2017, ARA&A, 55, 303
Kaspi S., Smith P. S., Netzer H., Maoz D., Jannuzi B. T., Giveon U., 2000, ApJ, 533, 631
King A., 2003, ApJ, 596, L27
Kitaki T., Mineshige S., Ohsuga K., Kawashima T., 2018, PASJ, 70, 108
Kubota A., Done C., 2018, MNRAS, 480, 1247 (KD18)
Lasota, J.-P., Vieira, R. S. S., Sadowski, A., Narayan, R., & Abramowicz, M. A. 2016, A&A, 587, A13
Mineshige S., Kawaguchi T., Takeuchi M., Hayashida K., 2000, PASJ, 52, 499
Mortlock D. J., et al., 2011, Natur, 474, 616
Novikov I. D., Thorne K. S., 1973, blho.conf, 343
Petrucci P.-O., Ursini F., De Rosa A., Bianchi S., Cappi M., Matt G., Dadina M., Malzac J., 2018, A&A, 611, A59
Porquet D., et al., 2019, A&A, 623, A11
Pounds K. A., Done C., Osborne J. P., 1995, MNRAS, 277, L5
Poutanen J., Lipunova G., Fabrika S., Butkevich A. G., Abolmasov P., 2007, MNRAS, 377, 1187
Puchnarewicz E. M., Mason K. O., Siemiginowska A., Fruscione A., Comastri A., Fiore F., Cagnoni I., 2001, ApJ, 550, 644
Remillard R. A., McClintock J. E., 2006, ARA&A, 44, 49
Sądowski A. PhD thesis 2011
Shakura N. I., Sunyaev R. A., 1973, A&A, 24, 337
Shapiro S. L., 2005, ApJ, 620, 59
Steinhardt C. L., Elvis M., 2010, MNRAS, 406, L1
Schulze, A., Done, C., Lu, Y., Zhang, F., & Inoue, Y. 2017, ApJ, 849, 4
Tang, J.-J., Goto, T., Ohyama, Y., et al. 2017, MNRAS, 466, 4568
Tang, J.-J., Goto, T., Ohyama, Y., et al. 2019, MNRAS, 484, 2575
Vestergaard M., Peterson B. M., 2006, ApJ, 641, 689
Vierdayanti, K., Sadowski, A., Mineshige, S., & Bursa, M. 2013, MNRAS, 436, 71
Volonteri, M., & Rees, M. J. 2005, ApJ, 633, 624
Wang, J.-M., Qiu, J., Du, P., & Ho, L. C. 2014, ApJ, 797, 65
Watarai K.-y., Fukue J., Takeuchi M., Mineshige S., 2000, PASJ, 52, 133
Wilms J., Allen A., McCray R., 2000, ApJ, 542, 914
Wise J. H., Regan J. A., O'Shea B. W., Norman M. L., Downes T. P., Xu H., 2019, Natur, 566, 85
Woo J.-H., Urry C. M., 2002, ApJ, 579, 530
Xie X., Shao Z., Shen S., Liu H., Li L., 2016, ApJ, 824, 38
Zhang, S. N., Cui, W., & Chen, W. 1997, ApJ, 482, L155

This paper has been typeset from a TEX/LATEX file prepared by the author.